The trimorphism of 3-Hydroxybenzoic acid: an experimental and computational study

Doris E. Braun

Electronic Supporting Information

1 COMPUTATIONAL 2
1.1 Low-energy conformations of 3-hydroxybenzoic acid 2
1.2 Computational generation of the crystal energy landscape 3
1.3 Packing comparison of the experimental and hypothetical low-energy crystal structures 7
1.4 Pairwise intermolecular energy calculations 11
1.5 Optimisation of the RT structure models (PBE-TS) 13
2 EXPERIMENTAL 14
2.1 Materials and Methods 14
2.2 Powder X-ray diffraction 16
2.3 Rietveld refinement 19
2.4 Structure of Form III 21
2.5 Solution calorimetry 23
2.6 Semi-schematic energy temperature diagram 25
2.7 Variable temperature IR spectroscopy 26
3 REFERENCES 28

1 COMPUTATIONAL

1.1 Low-energy conformations of 3-hydroxybenzoic acid

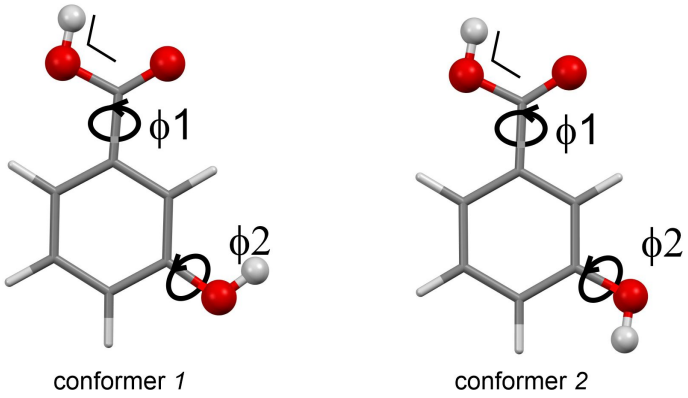

Figure S1. Molecular diagram of 3-hydroxybenzoic acid (3HBA). The torsions and the angle that were optimised within the crystal energy minimisations are highlighted. The two conformations were calculated to differ by 3.25 and 3.26 kJ mol^{-1} at the PBE0/6-31G(d,p) and PBE0/aug-cc-pVTz level of theory, respectively, with *conformer 1* being the global minimum conformation of 3HBA.

1.2 Computational generation of the crystal energy landscape

The crystal energy landscape of 3-hydroxybenzoic acid (Z′=1 and Z′=2), based on each of the two planar conformations, was generated with the program CrystalPredictor,[1-3] using a low-discrepancy sequence to search the crystal packing space with quasi-random values for unit cell dimensions, molecular orientations and positions, followed by rigid-molecule lattice energy minimisation. For each of the searches crystal structures were generated in 61 common space groups (*P*1, *P*-1, *P*2$_1$, P2$_1$/*c*, *P*222$_1$, *P*2$_1$2$_1$2, *P*2$_1$2$_1$2$_1$, *Pna*2$_1$, *Pca*2$_1$, *Pbca*, *Pbcn*, *C*2/*c*, *Cc*, *C*2, *Pc*, *Cm*, *P*2$_1$/*m*, *C*2/*m*, *P*2/*c*, *C*222$_1$, *Pmn*2$_1$, *Cmc*2$_1$, *Aba*2, *Fdd*2, *Iba*2, *Pnna*, *Pccn*, *Pbcm*, *Pnnm*, *Pmmn*, *Pnma*, *Pba*2, *Cmcm*, *Cmca*, *Fddd*, *Ibam*, *P*4$_1$, *P*4$_3$, *I*-4, *P*4/n, *P*4$_2$/*n*, *I*4/*m*, *I*4$_1$/*a*, *P*4$_1$2$_1$2, *P*4$_3$2$_1$2, *P*-42$_1$*c*, *I*-42*d*, *P*3$_1$, *P*3$_2$, *R*3, *P*-3, *R*-3, *P*312$_1$, *P*322$_1$, *R*3*c*, *R*-3*c*, *P*6$_1$, *P*6$_3$, *P*6$_3$/*m*, *P*213, *Pa*-3). In all searches the molecules were in a general position and held rigid. Searches were continued until 250,000 structures had been energy minimised for Z′=1 and 700,000 for Z′=2. The model for the intermolecular forces was an isotropic atom-atom potential (FIT) and atomic charges fitted to the PBE0/aug-cc-pVTz electrostatic potential using the CHELPG scheme.[4]

Following each CrystalPredictor search, the lowest energy structures, all those within 25 kJ mol^{-1} (Z′=1) or 12.5 kJ mol^{-1} (Z′=2) range with respect to that search minimum, were used as starting points for lattice energy minimisations (DMACRYS[5]) using distributed multipoles[6, 7] derived from the PBE0/aug-cc-pVTz charge densities and the FIT parameters[8] for the repulsion-dispersion energy. The conformations were still kept rigid.

The 532 most stable structures were refined allowing the conformational flexibility to optimise the proton positions, the COOH torsion (ϕ1), *m*-OH torsion (ϕ2) and COH (acid) angle (Figure S1), using the CrystalOptimizer database method.[9] All molecular structures and energies were calculated at the PBE0/6-31G(d,p) level of theory. The intermolecular lattice energies were evaluated form the PBE0/aug-cc-pVTz wave function distributed multipoles and the FIT potential[8] parameters for the repulsion-dispersion models. All isolated-molecule wave function calculations were performed using Gaussian16[10] and intermolecular lattice energies using DMACRYS.[5]

Helmholtz free energies[11] derived from the elastic constants[12] and *k*=0 phonons[13] calculated in the rigid-body harmonic approximation were estimated for the most stable structures at 298 K. This approximate Helmholtz free energy surface is referred to as the “crystal energy” and is reported in Fig. 2 (manuscript), with the relative energies for the low-energy structures at the intermediate stages given in Table S1.

Table S 1. The low-energy crystal structures of 3-hydroxybenzoic acid shown in Fig. 2. Experimental structures are indicated in bold.

C[a]	ID[b]	DMACRYS		Crystal-Optimizer		Crystal-Optimizer-FE		Space group	PI	Den-sity	Lattice parameters						Graph Set motif[c]
		E_{latt}	ΔE_{latt}	E_{latt}	ΔE_{latt}	E_{cry}	ΔE_{cry}				a	b	c	α	β	γ	
		/ kJ mol^{-1}								g cm^{-3}	/ Å			/ °			
1	**881 (I)**	**−97.65**	**0.00**	**−100.25**	**0.00**	**−114.20**	**0.00**	***P*2$_1$/*c***	**0.721**	**1.435**	**5.502**	**5.151**	**23.239**	**90**	**103.95**	**90**	**D**
1	**16 (II)**	**−96.87**	**0.78**	**−97.56**	**2.69**	**−113.61**	**0.58**	***Pna*2$_1$**	**0.722**	**1.435**	**20.522**	**3.699**	**8.423**	**90**	**90**	**90**	**C1**
1	74	−96.31	1.34	−97.45	2.81	−113.27	0.93	*P*2$_1$/*c*	0.721	1.429	22.426	7.447	3.886	90	81.74	90	C5
1	177	−96.28	1.37	−96.86	3.39	−113.22	0.97	*P*2$_1$2$_1$2$_1$	0.719	1.427	20.517	3.720	8.425	90	90	90	C1
1	117	−95.51	2.14	−96.72	3.53	−113.14	1.06	*P*2$_1$2$_1$2$_1$	0.721	1.433	3.798	22.513	7.489	90	90	90	C5
1	113	−94.85	2.80	−95.00	5.25	−113.12	1.08	*P*2$_1$2$_1$2$_1$	0.720	1.431	23.015	7.533	3.699	90	90	90	C5
1	9	−96.32	1.32	−96.95	3.30	−113.06	1.14	*P*2$_1$/*c*	0.733	1.439	3.740	8.422	20.389	90	83.24	90	C1
1	179	−94.48	3.17	−95.74	4.52	−112.88	1.32	*P*2$_1$/*c*	0.702	1.412	3.840	7.457	22.758	90	94.23	90	C5
1	**111 (III)**	**−96.90**	**0.75**	**−98.48**	**1.77**	**−112.19**	**2.01**	***P*2$_1$/*c***	**0.747**	**1.470**	**9.440**	**8.430**	**7.864**	**90**	**85.51**	**90**	**C1**
1	6	−96.50	1.15	−97.25	3.00	−112.07	2.13	*P*2$_1$	0.707	1.444	11.824	8.422	3.709	90	120.67	90	C1
1	23	−93.32	4.33	−94.55	5.70	−112.01	2.19	*P*2$_1$/*c*	0.732	1.457	3.774	7.490	22.354	90	85.49	90	C2
1	413	−94.90	2.75	−95.52	4.73	−111.96	2.24	*P*2$_1$/*c*	0.715	1.426	3.685	20.746	9.088	90	67.87	90	C2
1	39	−96.76	0.89	−97.81	2.44	−111.89	2.31	*P*2$_1$	0.719	1.437	11.082	7.452	3.887	90	84.16	90	C5
1	137	−94.25	3.39	−94.71	5.54	−111.84	2.35	*C*2/*c*	0.702	1.397	16.425	3.711	21.869	90	80.18	90	C3
1	30	−94.33	3.32	−95.11	5.14	−111.82	2.38	*P*2$_1$/*c*	0.716	1.432	3.689	8.421	20.805	90	97.65	90	C2
1	156	−94.27	3.38	−94.88	5.38	−111.74	2.46	*P*2$_1$/*c*	0.712	1.417	8.429	3.709	23.437	90	62.09	90	C2
1	24	−95.59	2.06	−96.99	3.26	−111.47	2.73	*P*2$_1$/*c*	0.734	1.452	10.230	8.421	7.692	90	72.46	90	C1
1	15	−95.06	2.59	−95.66	4.59	−111.29	2.90	*P*2$_1$/*c*	0.708	1.409	10.943	3.705	16.413	90	101.96	90	C3
1	705	−97.56	0.09	−97.73	2.52	−111.01	3.19	*P*2$_1$/*c*	0.730	1.447	5.299	5.520	21.711	90	86.85	90	D
1	40	−95.88	1.77	−96.19	4.06	−110.68	3.52	*P*2$_1$/*c*	0.707	1.432	12.015	8.423	7.165	90	62.07	90	C1
1	110	−95.34	2.31	−95.97	4.28	−110.66	3.54	*P*2$_1$/*c*	0.721	1.435	7.086	8.432	10.935	90	78.05	90	C1
1	195	−94.14	3.51	−94.61	5.64	−110.63	3.57	*C*2/*c*	0.697	1.388	25.255	3.746	16.383	90	121.45	90	C3
1	352	−94.58	3.07	−95.13	5.12	−110.36	3.84	*P*-1	0.711	1.427	11.385	3.736	8.427	85.48	64.87	94.03	C2
1	494	−94.20	3.45	−94.37	5.88	−110.35	3.84	*P*2$_1$	0.712	1.422	7.523	3.682	11.906	90	78.08	90	C5

C[a]	ID[b]	DMACrys		Crystal-Optimizer		Crystal-Optimizer-FE		Space group	PI	Den-sity	Lattice parameters						Graph Set group
		E_{latt}	ΔE_{latt}	E_{latt}	ΔE_{latt}	E_{cry}	ΔE_{cry}				a	b	c	α	β	γ	
		/ kJ mol^{-1}								g cm^{-3}	/ Å			/ °			
12	716	−94.38	3.27	−96.48	3.77	−110.24	3.95	$P2_1/c$	0.717	1.426	11.090	5.029	23.873	90	75.05	90	D
1	201	−94.78	2.87	−95.00	5.25	−110.20	4.00	$P2_1/c$	0.724	1.431	15.169	3.778	11.593	90	74.79	90	C4
1	95	−95.63	2.02	−95.80	4.45	−110.19	4.01	$P2_1/c$	0.735	1.453	6.810	4.983	18.621	90	91.88	90	C2
1	135	−95.28	2.37	−95.55	4.70	−110.17	4.02	$P2_1/c$	0.711	1.423	11.296	8.406	7.179	90	71	90	C1
12	825	−94.24	3.41	−96.00	4.25	−110.10	4.09	$P2_1$	0.716	1.417	23.073	5.073	5.531	90	88.92	90	D
1	144	−95.84	1.81	−95.87	4.38	−110.10	4.10	$P4_32_12$	0.710	1.404	5.953	5.953	36.879	90	90	90	C1
1	252	−94.76	2.89	−94.84	5.41	−109.80	4.40	$Pna2_1$	0.718	1.430	22.938	3.717	7.528	90	90	90	C1
1	835	−95.81	1.84	−95.95	4.30	−109.76	4.44	$P2_1/c$	0.730	1.436	5.491	5.247	22.583	90	79.00	90	D
1	174	−94.01	3.64	−94.63	5.62	−109.62	4.58	$P2_1/c$	0.716	1.424	7.850	8.452	9.767	90	83.72	90	C1
12	1118	−91.39	6.26	−95.15	5.10	−109.50	4.69	P-1	0.698	1.395	7.976	7.881	11.839	88.32	102.22	65.77	D
1	168	−93.06	4.59	−94.38	5.87	−109.46	4.74	$P2_12_12_1$	0.721	1.408	8.413	10.994	7.045	90	90	90	C1
1	215	−93.43	4.22	−94.73	5.52	−109.42	4.78	$C2/c$	0.732	1.441	9.026	8.404	16.820	90	86.27	90	C1
1	194	−92.36	5.29	−94.29	5.96	−109.40	4.80	$P2_12_12_1$	0.727	1.422	8.418	11.033	6.948	90	90	90	C1
1	121	−93.81	3.84	−94.46	5.79	−109.19	5.01	$P2_12_12_1$	0.711	1.421	11.389	8.427	6.728	90	90	90	C1
1	448	−90.83	6.81	−94.25	6.00	−109.01	5.19	$C2/c$	0.717	1.421	20.089	8.459	8.015	90	108.57	90	C2
1	1050	−94.48	3.17	−94.97	5.28	−108.81	5.38	$C2/c$	0.691	1.370	25.796	3.800	13.865	90	80.21	90	D
1	238	−93.84	3.81	−94.55	5.70	−108.72	5.48	Cc	0.691	1.382	3.671	21.492	8.436	90	85.82	90	C1
1	1021	−94.71	2.94	−95.54	4.71	−108.36	5.83	$P2_1/c$	0.689	1.372	8.218	6.880	12.961	90	65.85	90	D
1	1005	−94.39	3.26	−94.48	5.77	−108.19	6.01	$P2_1/c$	0.682	1.358	12.381	3.921	13.984	90	84.45	90	D
1	184	−94.18	3.47	−94.50	5.75	−108.03	6.16	$P2_1$	0.725	1.429	7.618	8.439	5.019	90	84.09	90	C1
1	287	−94.18	3.47	−94.31	5.94	−107.84	6.36	$P2_1/c$	0.697	1.392	11.211	8.436	8.009	90	60.48	90	C1

[a]Conformer *1* (Z'=1) or *12* (Z'=2). [b]Rank according to CrystalPredictor search. [c]For graph set motifs see Fig. 3 of the manuscript.

The quality of the reproduction of the experimental forms was quantified using the overlay[14] of a 15 molecule cluster, $rmsd_{15}$, as calculated using the Molecular Similarity Module in Mercury.

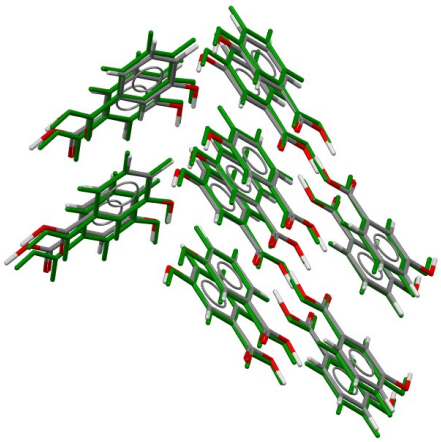

Figure S2. Overlay of the 15-molecule cluster of the observed structure of **Form I** (BIDLOP, coloured by element) and calculated structure (in green), $rmsd_{15}$=0.217 Å.

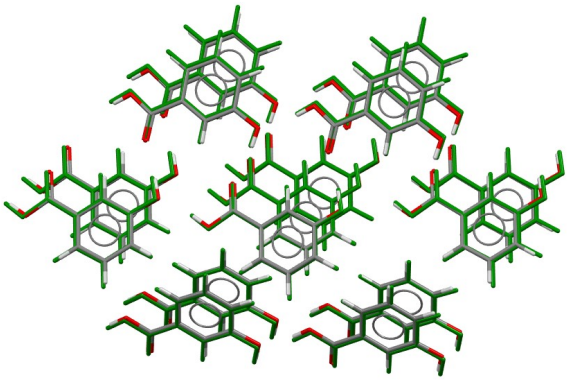

Figure S3. Overlay of the 15-molecule cluster of the observed structure of **Form II** (BIDLOP02, coloured by element) and calculated structure (in green), $rmsd_{15}$=0.139 Å.

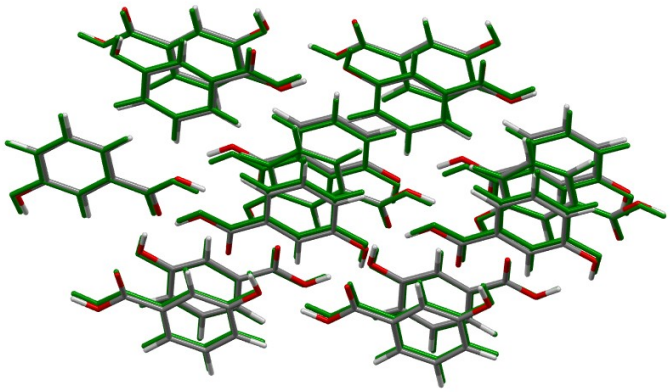

Figure S4. Overlay of the 15-molecule cluster of the observed structure of **Form III** (coloured by element) and calculated structure (in green), $rmsd_{15}$=0.196 Å.

1.3 Packing comparison of the experimental and hypothetical low-energy crystal structures

Crystal packing comparisons were performed using the program CrystalCMP[15] with a cluster size of 15 3-hydroxybenzoic acid molecules.

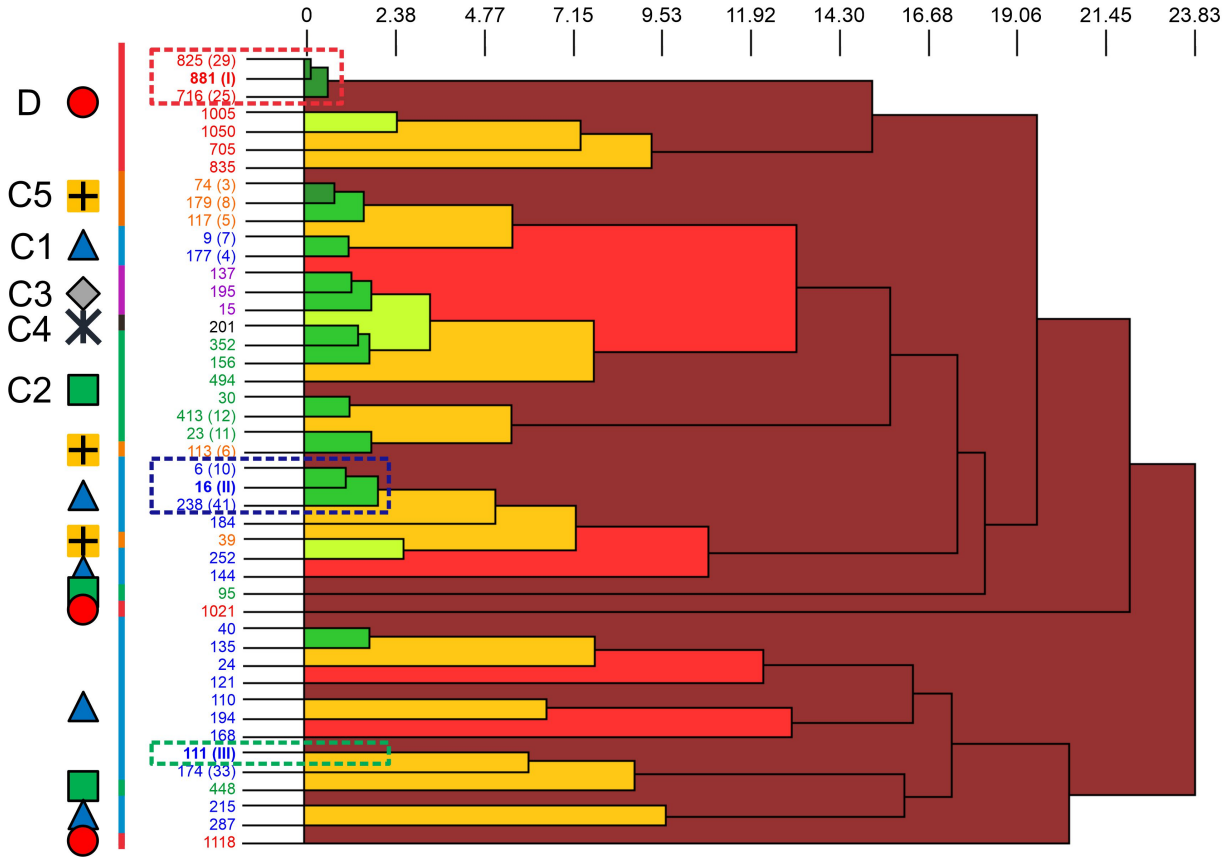

Figure S5. The Dendrogram shows the packing similarity of experimental and computed 3HBA structures. In the dendrograms the horizontal axis corresponds to the PS_{ab} value (similarity). In this case, dark green indicates almost identical packing and dark red indicates dissimilar packing. PS_{ab} values are given in Figure S6. Symbols and colour coding of the vertical axis are according to hydrogen-bonding motifs (see Fig. 3 of the manuscript). Numbers correspond to the CrystalPredictor rank and numbers in parenthesis to either the experimental forms (I, II, III) or to the rank of lowest-energy structures in Fig. 2 of the manuscript.

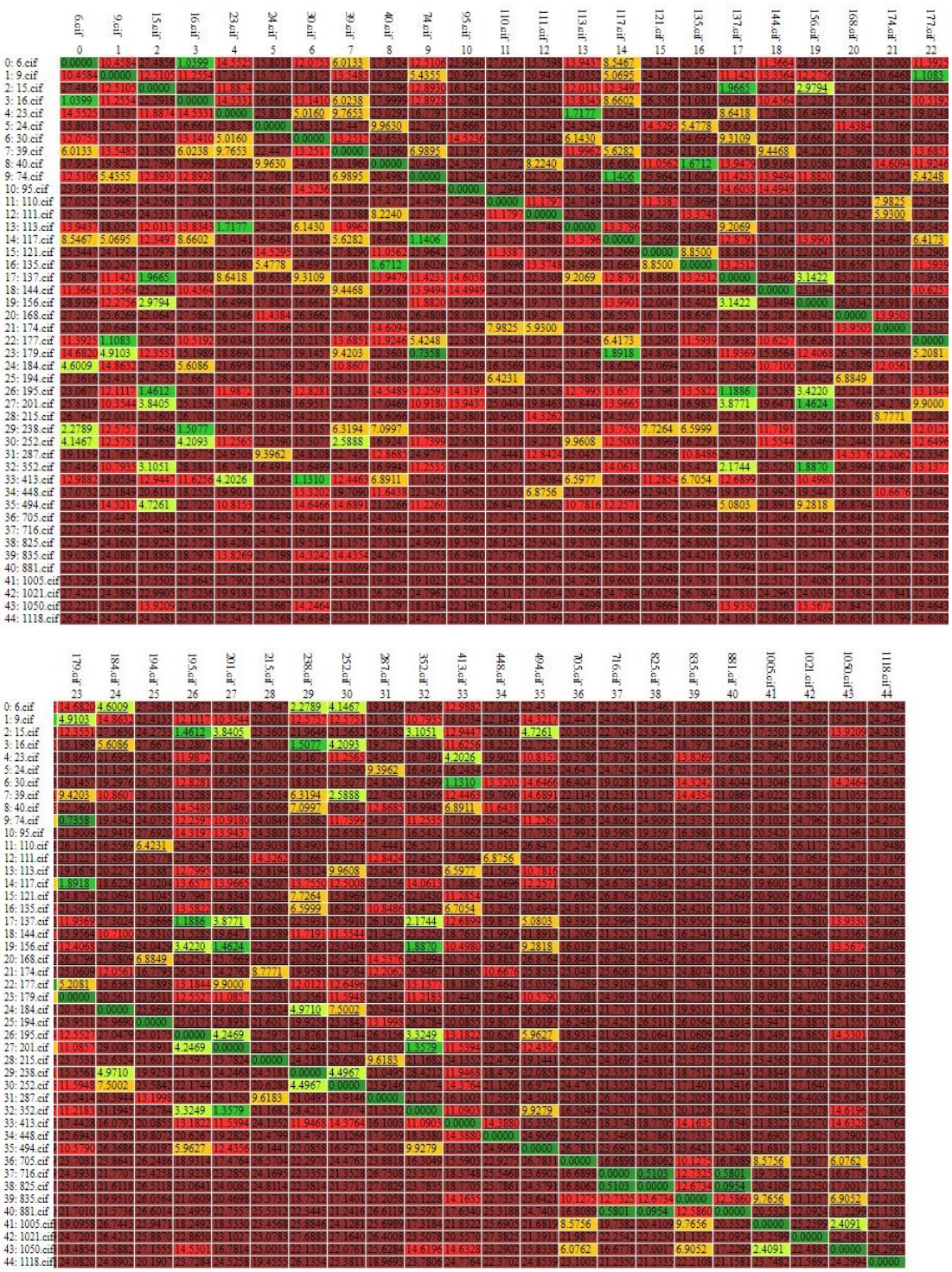

Figure S6. Similarity matrix of experimental and computed 3HBA structures.

Packing comparison of cluster 881(Form I) – 716 – 825

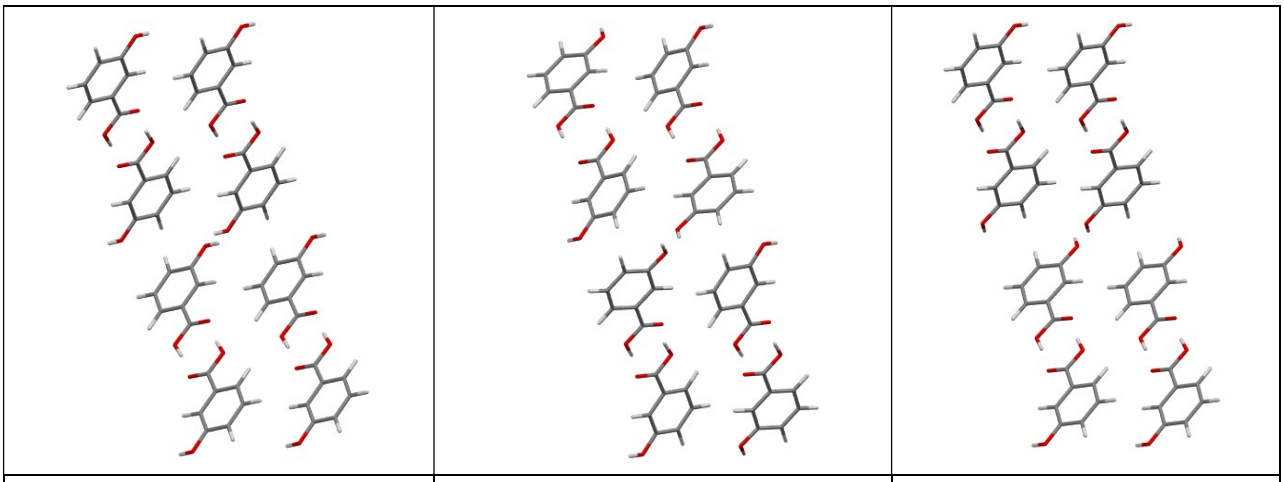

881 (Form I)	716	825

Figure S7. Packing comparison of Form I and isostructural packing arrangements differing only in the orientation of the *m*-OH group. Note that structure 716 can be "transformed" to a disordered Z'=1 structure. The experimental form is an ordered Z'=1 structure.

Packing comparison of cluster 16 (Form II) – 6 – 238

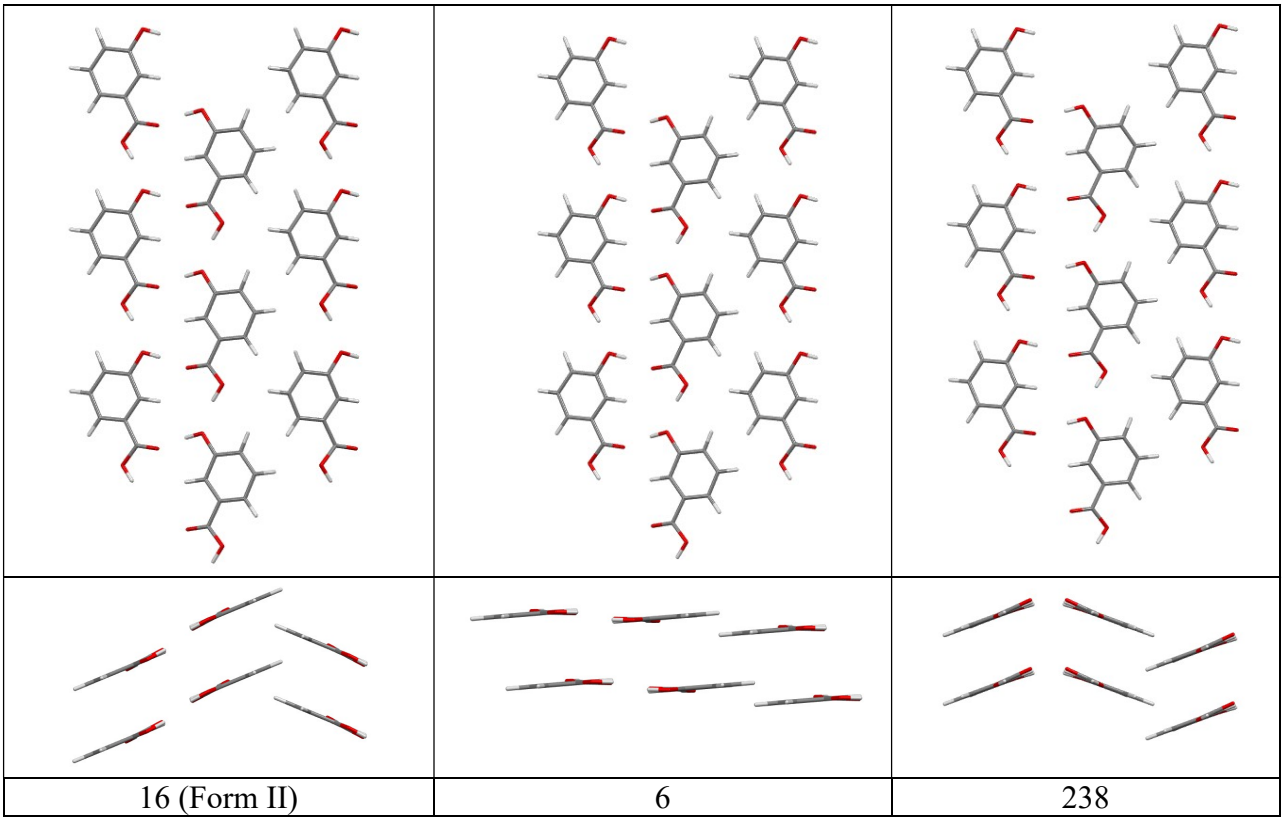

16 (Form II)	6	238

Figure S8. Packing comparison of Form II and structurally related hypothetical packings.

Packing comparison of cluster 111 (Form III) – 174

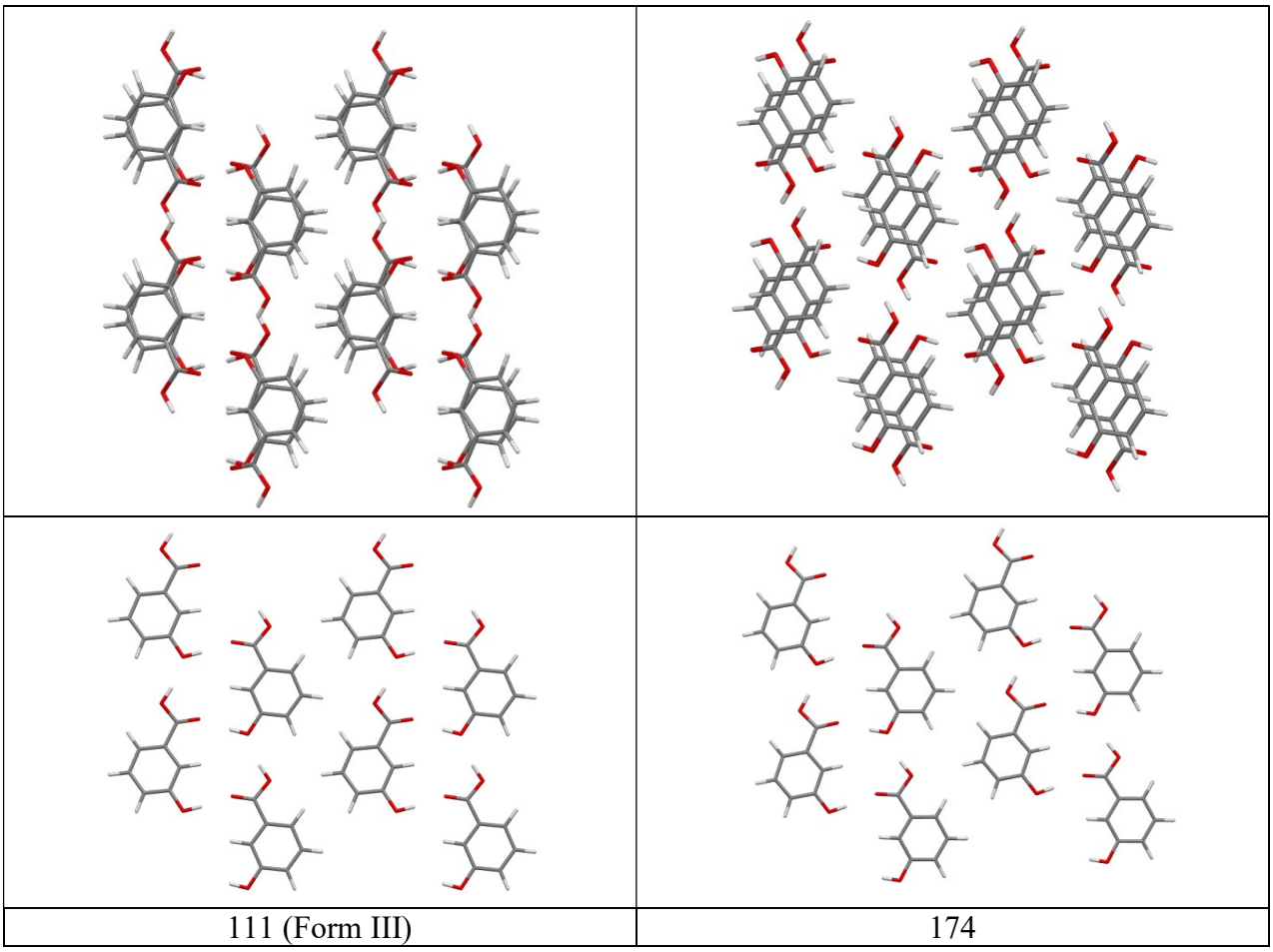

Figure S9. Packing comparison of Form III and the hypothetical structure 174. The two structures exhibit identical layers which are differently stacked.

1.4 Pairwise intermolecular energy calculations

Pairwise energy contributions were calculated using CrystalExplorer V17.[16-18] The optimised atomic positions (PBE-TS, lattice parameters fixed to experimental values) were used for the calculations (radius 3.8 Å). The model energies have been calculated between all unique nearest neighbour pairs. The used model (CE-B3LYP) uses B3LYP/6-31G(d,p) molecular wave functions calculated by applying the molecular geometries extracted from the crystal structures. This approach uses electron densities of unperturbed monomers to obtain four separate energy components: electrostatic (E_E), polarisation (E_P), dispersion (E_D), and exchange-repulsion (E_R). Each energy term was scaled independently to fit a large training set of B3LYP-D2/6-31G(d,p) counterpoise-corrected energies from both organic and inorganic crystals.[18]

Table S2. Overview of stabilising pairwise energetic contributions[a] for 3HBA forms I-III.

Interaction (times present)	Distance (Å)	E_E (kJ mol^{-1})	E_P (kJ mol^{-1})	E_D (kJ mol^{-1})	E_R (kJ mol^{-1})	E_{tot}[b] (kJ mol^{-1})	*notes*
Form I, $E_{cluster}$ = −120.3 kJ mol^{-1}							
1 (1)	7.74	−151	−35	−12.7	197	−74.9	R2,2(8)
2 (2)	7.37	−38.6	−8.1	−10.1	43.2	−29	OH···O
3 (1)	5.67	−4.2	−1	−15.9	5.9	−15.3	aromatic
4 (2)	4.94	−2.5	−1.1	−21.8	12.6	−14.7	aromatic
5 (2)	5.49	−2.9	−0.7	−13.8	6.5	−11.7	aromatic
6 (2)	7.39	−4.5	−2	−6	5.8	−7.9	
7 (2)	6.76	−2	−0.4	−10.3	6.1	−7.6	
8 (1)	6.96	−2.7	−0.9	−11	12.6	−5.3	
9 (1)	8.73	−1.5	−0.2	−1.9	0.1	−3.3	
Form II, $E_{cluster}$ = −113.7 kJ mol^{-1}							
1 (2)	6.75	−59.3	−13.4	−10.9	67.5	−40.3	OH···O(acid)
2 (2)	8.29	−53.5	−10.7	−9.7	67.2	−31.4	OH(acid) ···O
3 (2)	3.76	−1.5	−1.2	−32.9	19.1	−19.3	aromatic
4 (2)	7.04	−3.9	−0.5	−10.3	8.2	−8.4	aromatic
5 (2)	6.36	−0.5	−1.1	−8.4	2.2	−7.3	
6 (2)	7.04	−1.3	−0.2	−8.4	4.1	−6.3	
7 (2)	9.11	0.5	−0.1	−1.4	0	−0.7	
Form III, $E_{cluster}$ = −117.7 kJ mol^{-1}							
1 (2)	6.71	−64.7	−14.7	−11.4	79.3	−40.2	OH···O(acid)
2 (2)	8.3	−51.1	−10.3	−9.7	62.9	−31.2	OH(acid) ···O
3 (2)	4.01	−0.3	−1.1	−29.8	16	−17.2	aromatic
4 (1)	6.91	−5	−0.8	−8.1	2.1	−11.6	aromatic
5 (1)	7.30	−3.8	−0.3	−10.8	7.5	−9	
6 (1)	5.98	0	−0.2	−11.9	5	−7.5	
7 (2)	7.41	−2	−0.4	−10.2	7.1	−6.9	
8 (1)	5.50	3.8	−1.7	−13.9	6.2	−5.5	
9 (2)	8.21	−2.9	−0.3	−2.6	0.1	−5.4	

[a]Electrostatic (E_E), polarisation (E_P), dispersion (E_D) and exchange-repulsion energy (E_R) contributions. [b]$E_{tot} = k_E E_E + k_P E_P + k_D E_D + k_R E_R$, with k being scale factors.[18]

The energy framework diagrams for forms I, II and III of 3HBA are given in Figure S10 - Figure S12. Note that only the strongest pairwise interactions (< 10 kJ mol^{-1}) are shown.

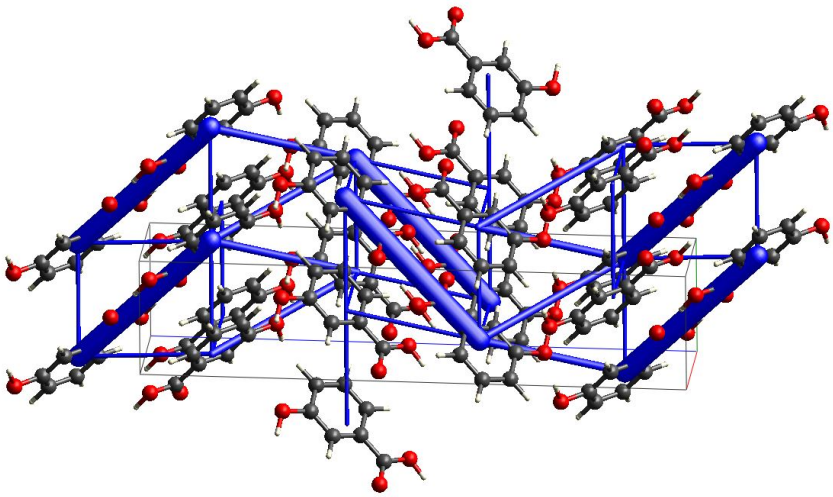

Figure S10. Energy framework diagram (total energy) for 3HBA form I viewed along the *a* crystallographic axis. The energy scale factor is 60. Stabilising contacts are shown in blue. The thickness corresponds to the strength. Pairwise interaction energies < 10 kJ mol^{-1} are omitted.

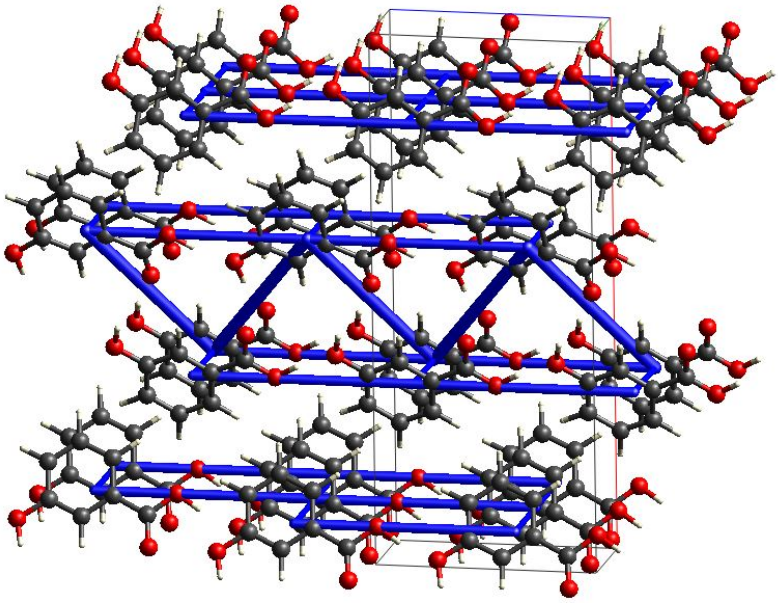

Figure S11. Energy framework diagram (total energy) for 3HBA form II viewed along the *b* crystallographic axis. The energy scale factor is 60. Stabilising contacts are shown in blue. The thickness corresponds to the strength. Pairwise interaction energies < 10 kJ mol^{-1} are omitted.

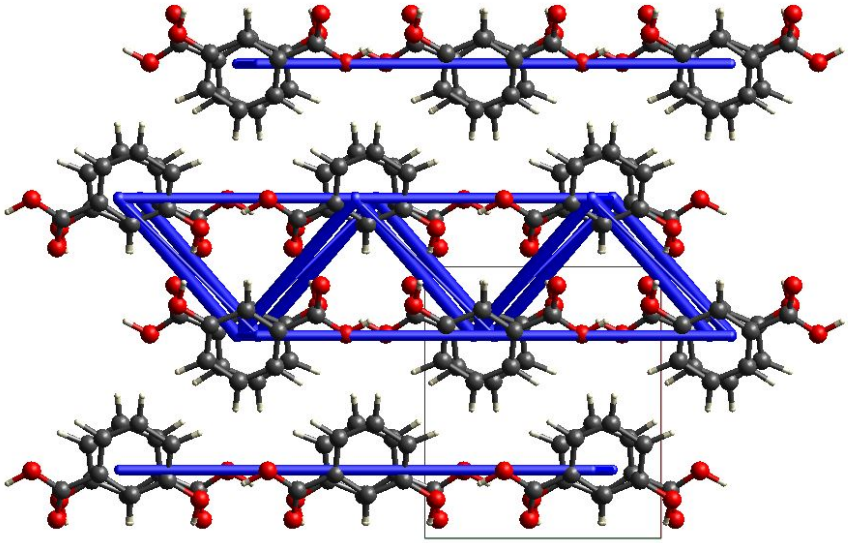

Figure S12. Energy framework diagram (total energy) for 3HBA form III viewed along the *c* crystallographic axis. The energy scale factor is 60. Stabilising contacts are shown in blue. The thickness corresponds to the strength. Pairwise interaction energies < 10 kJ mol^{-1} are omitted.

1.5 Optimisation of the RT structure models (PBE-TS)

Structures 16 (II), 111 (III) and 811 (I) were reoptimised, using the RT lattice parameters derived from the single crystal structures or form indexing the form III powder pattern, with periodic density functional calculations (CASTEP[19]). The Perdew-Burke-Ernzerhof (PBE) generalised gradient approximation (GGA) exchange-correlation density functional[20] and ultrasoft pseudopotentials,[21] with the addition of the Tkatchenko and Scheffler (TS)[22] semi-empirical dispersion correction, were applied. The number of *k*-points were chosen to provide a maximum spacing of 0.07 $Å^{-1}$ and a basis set cut-off of 780 eV was applied. The optimisations were considered complete when energies were converged to better than $2x10^{-5}$ eV per atom, atomic displacements converged to $1x10^{-3}$ Å, and maximum forces to $5x10^{-2}$ eV $Å^{-1}$.

2 EXPERIMENTAL

2.1 Materials and Methods

Materials

3-Hydroxybenzoic acid (form I) was obtained from Dr. Theodor Schuchardt.

Preparation of the polymorphs

Forms I and II were prepared by recrystallising the compound from a hot-saturated ethanol and ethyl acetate solution (saturated at the boiling point of the solvent), respectively.

Form III was obtained from the quench cooled melt of 3HBA. In case the melt was cooled too slowly form I seeds were present due to the fact that 3HBA sublimes (form I) at temperatures > 150 °C.

Differential scanning calorimetry

DSC thermograms were recorded on a DSC 7 (Perkin-Elmer Norwalk, Ct., USA) controlled by the Pyris 8.0 software. Using a UM3 ultramicrobalance (Mettler, Greifensee, CH), samples of approximately 3 – 5 mg were weighed into sealed aluminium capsules. The samples were heated using rates in between 5 and 10 °C min^{-1}, with dry nitrogen as the purge gas (purge: 20 ml min^{-1}). The instrument was calibrated for temperature with pure benzophenone (mp 48.0 °C) and caffeine (236.2 °C), and the energy calibration was performed with indium (mp 156.6 °C, heat of fusion 28.45 Jg^{-1}). The errors on the stated temperatures and enthalpy values were calculated at the 95% confidence intervals and are based on at least five measurements.

Solution calorimetry

The experiments were performed with the TAM III microcalorimeter unit (TA Instruments, Eschborn, Germany). Solution calorimetry data were recorded using a [3220]-20 mL micro solution ampoule. The experiments were performed at 25 °C in 15 mL of DMSO. Approximately 10 to 15 mg of sample was accurately weighed into reusable stainless-steel cartridges using a UM3 ultramicrobalance (Mettler, Greifensee, Switzerland). Once the baseline had stabilised to ± 50 nW, the capsule was dropped into the calorimeter. The heat flow into or out of the calorimeter was recorded and data analysis performed using the TAM Assistant software. The heat flow of the empty ampoule was subtracted from the heat flow of the sample measurements. The errors on the stated enthalpy values are calculated at the 95% confidence intervals and are based on at least three measurements. The calorimeter was calibrated using the electrical substitution method and with reference materials (KCl and sucrose).

Infrared spectroscopy

Infrared spectra were recorded with a diamond ATR (PIKE GaldiATR, Madison, US) crystal on a Bruker Vertex 70 FTIR spectrometer (Bruker Analytische Messtechnik GmbH, Germany). The spectra were recorded between 4000 and 400 cm^{-1} at an instrument resolution of 2 cm^{-1} (32 scans per spectrum).

Powder X-ray diffraction

PXRD patterns were obtained using an X'Pert PRO diffractometer (PANalytical, Almelo, NL) equipped with a θ/θ coupled goniometer in transmission geometry, programmable XYZ stage with well plate holder, Cu-$K_{\alpha 1,2}$ radiation source and a solid state PIXcel detector. The patterns were recorded at a tube voltage of 40 kV and tube current of 40 mA, applying a step size of $2\theta =$ 0.013° with 80 s or 200 s per step in the 2θ range between 2° and 40°.

2.2 Powder X-ray diffraction

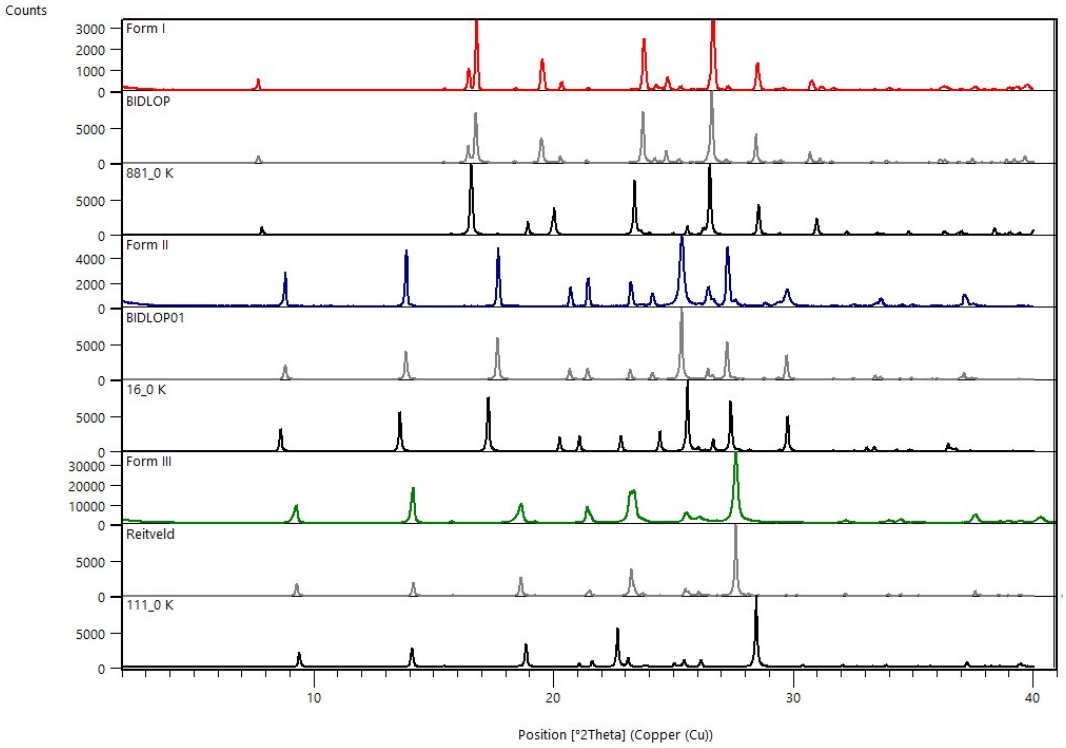

Figure S13. Comparison of experimental (red – I, blue – II, green – III), and simulated PXRD patterns (grey – from crystal structures, black – from computationally generated structures).

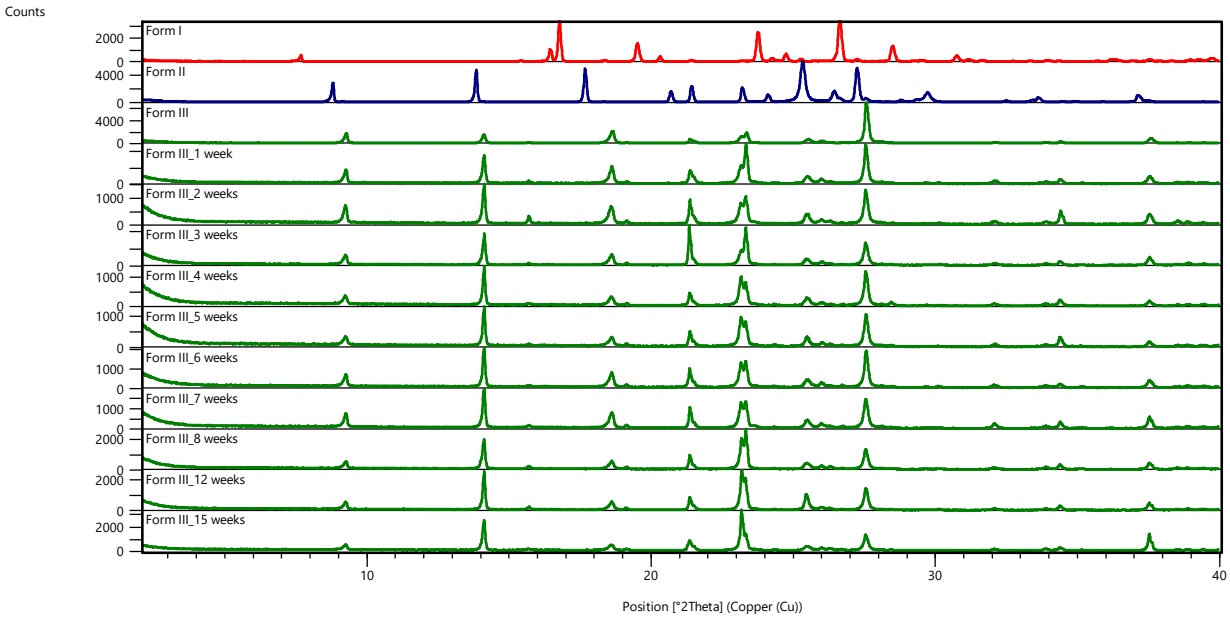

Figure S14. Form III storage experiments at ambient conditions. Form I and II reference patterns are given for comparison.

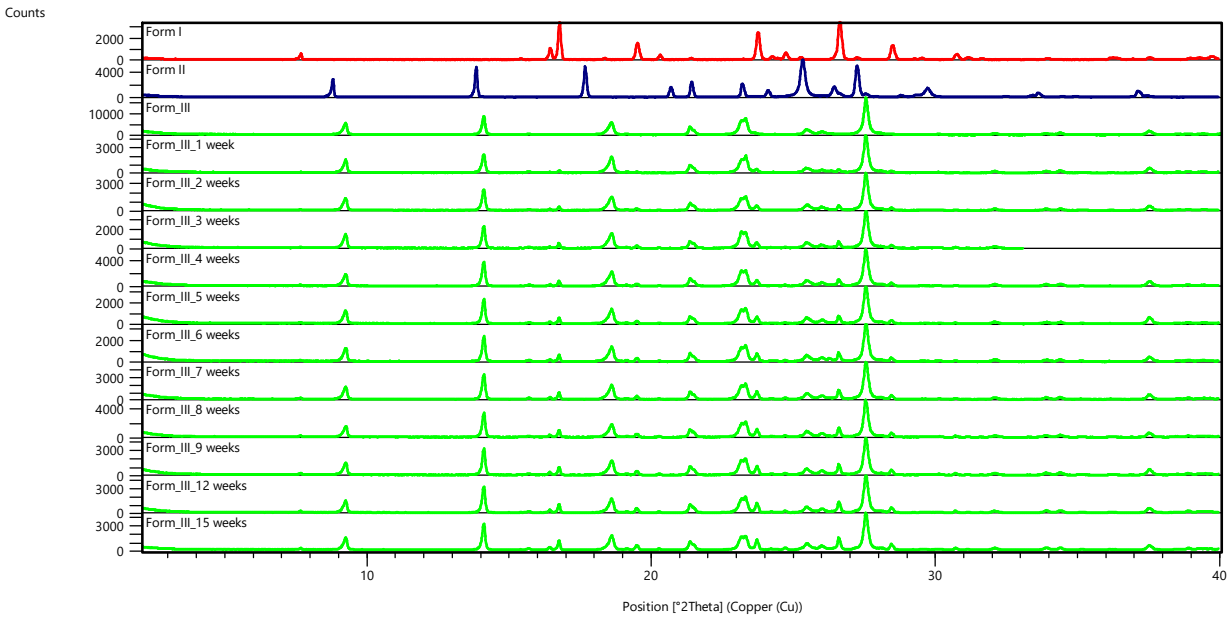

Figure S15. Form III (plus form I impurity) storage experiments at ambient conditions. Form I and II reference patterns are given for comparison.

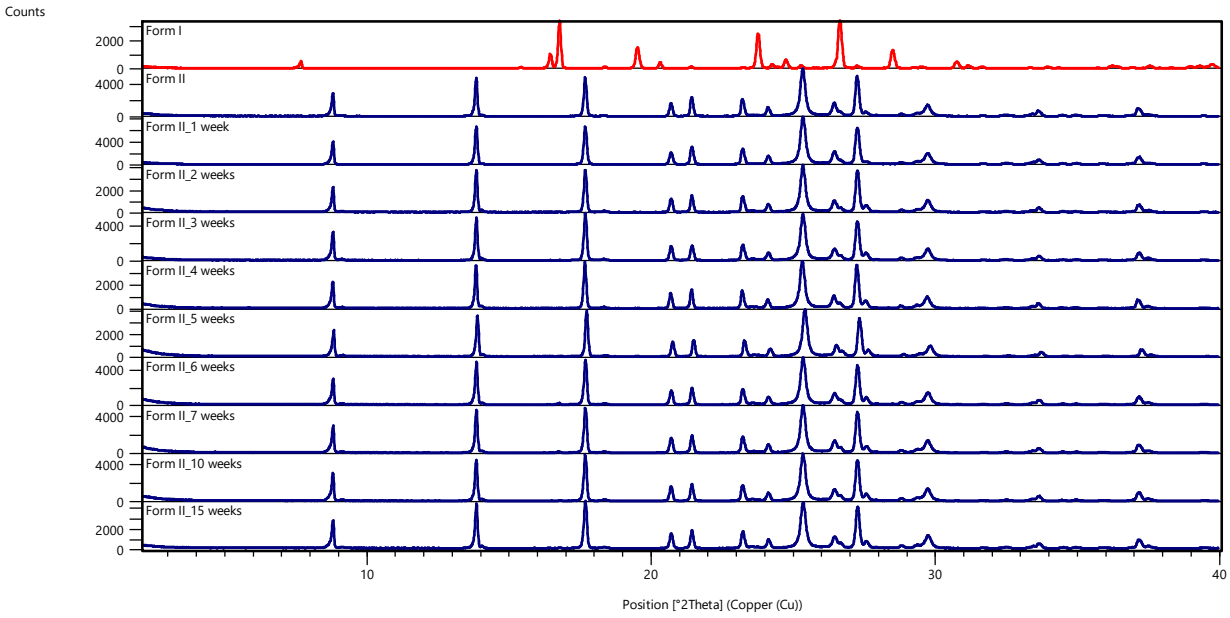

Figure S16. Form II storage experiments at ambient conditions. Form I reference patterns is given for comparison.

2.3 Rietveld refinement

3-Hydroxybenzoic acid form III was produced in DSC heating-cooling experiments. The sample was gently, but finely ground using a mortar and pestle. Due to the sample preparation (recrystallisation from the melt) preferred orientation could not be avoided. The data was recorded in transmission geometry as described in section 2.1. The pattern was recorded at a tube voltage of 40 kV and tube current of 40 mA, applying a step size of $2\theta = 0.007°$ with 3200 s per step in the 2θ range between 2° and 70°.

Form III indexed to a monoclinic unit cell,[23, 24] $P2_1/c$, with Z'=1. The data were background subtracted and truncated to 41.70° 2θ for Pawley fitting.[25] Simulated annealing was used to optimise the 3HBA model against the diffraction data set in direct space. The internal coordinate (Z-matrix) description was derived from the PBE-TS optimised Form III structure (see section 1.5). The structure was solved using 100 simulated annealing runs of 5×10^7 moves per run as implemented in DASH,[24] allowing 6 external and 1 internal degree (ϕ1 dihedral, Figure S1) of freedom. The best solution returned a χ^2 ratio of 3.06 (profile χ^2/ Pawley χ^2). This solution was then optimised again using CASTEP (for settings see section 1.5), with the lattice parameters fixed to the experimentally determined values. The two CASTEP optimisations were superimposable.

The minimised structure was then used as an input for Rietveld refinement, 2θ range 3.5 to 69.02°, using TOPAS academic V7.[26] The geometry of the acid molecule was defined by a rigid body. Rotation and translation parameters were simultaneously refined. The background was modelled by a set of consecutive points with refinable intensities. The isotropic temperature factor (B_{iso}) for non-hydrogen atoms refined to 3.91(9) and for hydrogen atoms to $1.2 \bullet B_{iso}$. The final refinement included a total of 50 parameters (26 profile, 4 cell, 1 scale, 12 preferred orientation, 1 isotropic temperature factor, 3 position and 3 rotation). The refinement converged at R_{wp} = 10.40%, R_{exp} = 1.76%, R_p = 8.17% (Figure S17).

The resulting structure from the Rietveld refinement was further scrutinised by allowing all coordinates to refine freely. As expected, the improvement (R_{wp}) came at the expense of some chemical sense (e.g. slight distortion in planarity of the aromatic ring, movement of H atoms to nonsensical positions), but otherwise, the geometry of the 3HBA molecule was well preserved, confirming the correctness of the rigid body refined crystal structure.

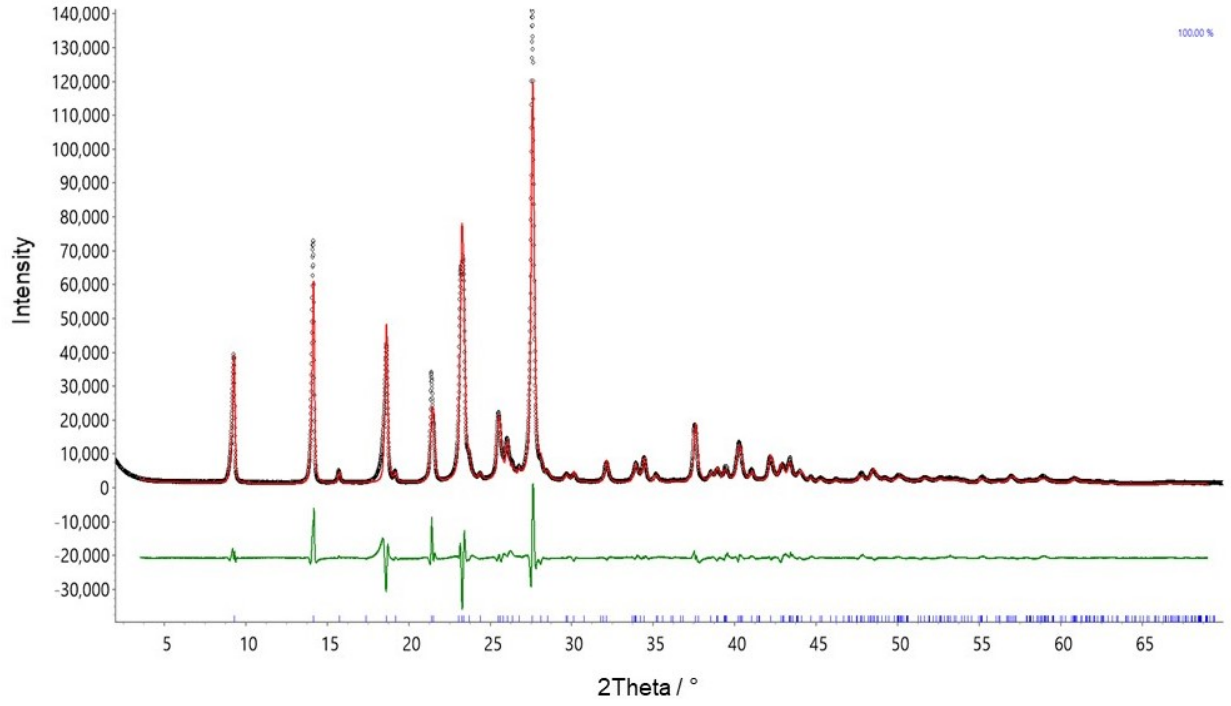

Figure S17. Observed (black points), calculated (red line) and difference (green line) profiles for the Rietveld refinement of Form III. Blue tick marks denote the peak positions.

To further check the correctness of the refinement a full structure optimisation in P1, incl. lattice parameters, was undertaken[27] using CASTEP. A comparison of the experimental structure and optimised structures (lattice parameters fixed to experimental values and full optimisation) are in excellent agreement ("RT": $rmsd_{15}$ = 0.047 Å and 0 K: $rmsd_{15}$ = 0.090 Å, Figure S18 & Figure S19).

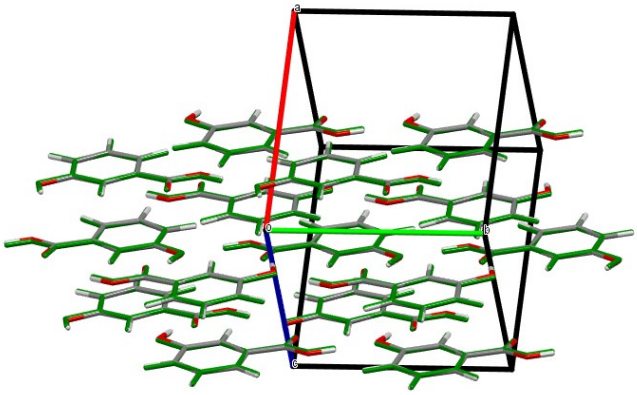

Figure S18. Overlay of the 15-molecule cluster of the observed structure of Form III (coloured by element) and calculated PBE-TS "RT" structure (in green), $rmsd_{15}$=0.047 Å.

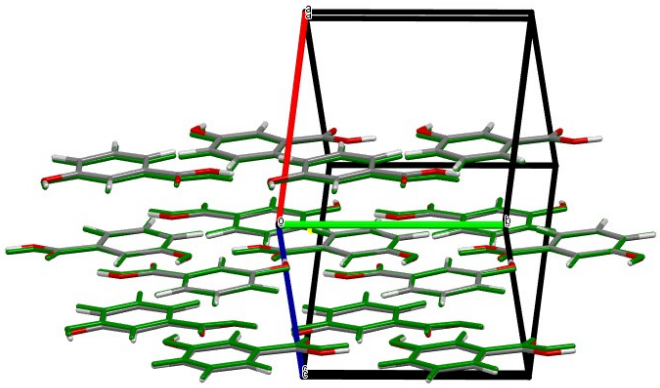

Figure S19. Overlay of the 15-molecule cluster of the observed structure of Form III (coloured by element) and calculated PBE-TS 0 K structure (in green), $rmsd_{15}$=0.090 Å.

2.4 Structure of Form III

```
TITL Form III
CELL 0.71073        9.6308      8.2989      7.7396      90      98.716      90
ZERR 4              0.0003      0.0002      0.0002      0       0.003       0
LATT 1
SYMM -x,1/2+y,1/2-z
SFAC  C      H      O
UNIT 28      24     12
FVAR 1.00
C1    1     0.1588(8)    0.2535(5)    0.4249(5)
C2    1     0.3711(9)    0.1368(7)    0.5869(8)
C3    1     0.2391(8)    0.1187(5)    0.4847(6)
C4    1     0.4223(10)   0.2912(7)    0.6282(9)
C5    1     0.3431(10)   0.4265(6)    0.5693(8)
C6    1     0.2112(9)    0.4074(5)    0.4671(6)
C7    1     0.1817(8)    -0.0423(5)   0.4330(5)
H1    2     0.2100(8)    -0.2703(5)   0.4646(6)
H2    2     0.0511(8)    0.5142(4)    0.3248(6)
H3    2     0.0570(8)    0.2390(4)    0.3445(5)
H4    2     0.4326(10)   0.0310(7)    0.6308(9)
H5    2     0.5252(10)   0.3066(8)    0.7065(11)
H6    2     0.3833(10)   0.5472(7)    0.6001(9)
O1    3     0.0736(7)    -0.0644(4)   0.3266(4)
O2    3     0.2560(9)    -0.1664(6)   0.5096(6)
O3    3     0.1363(9)    0.5434(5)    0.4095(6)
END
```

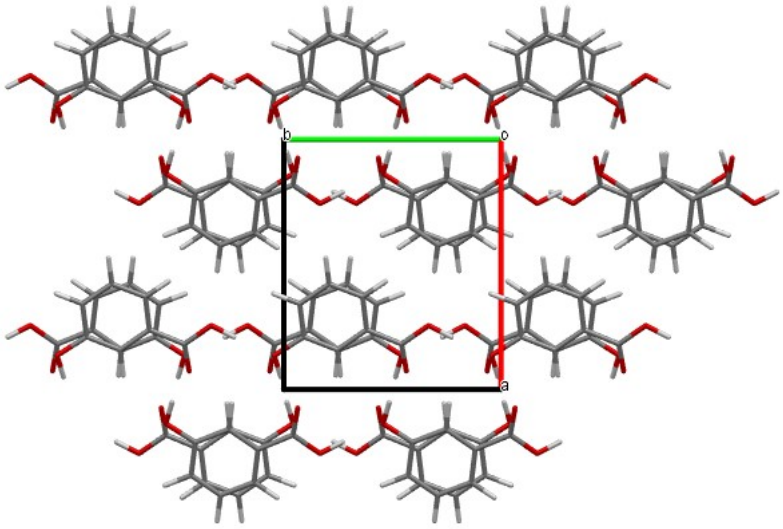

Figure S20. Packing diagram of form III viewed along the *c* crystallographical axis.

2.5 Solution calorimetry

Exemplarily, power-time curves are shown for each of the polymorphs and the empty cartridge (blank value).

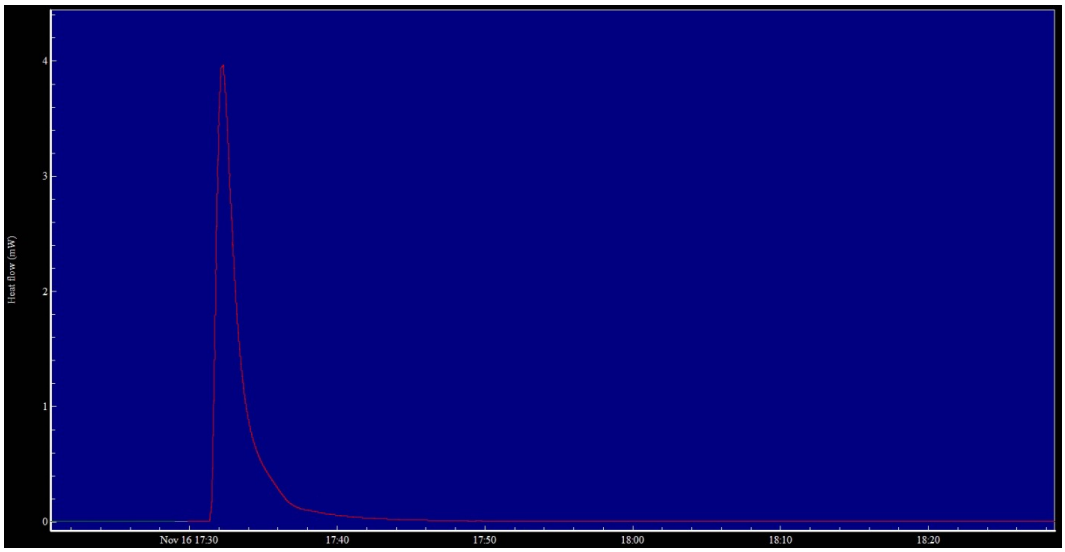

Figure S21. Power-time curve for 3HBA form I dissolution in DMSO.

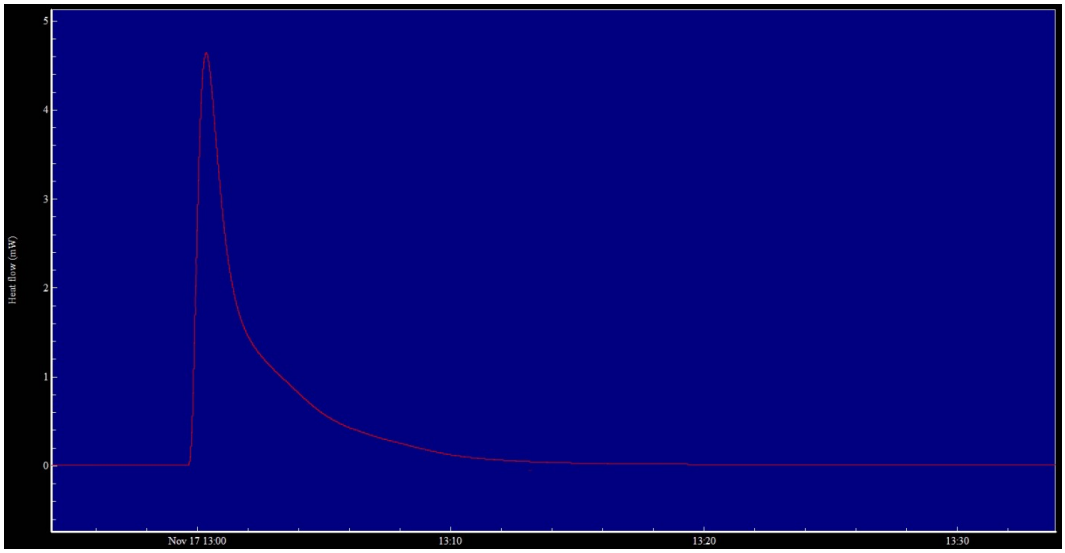

Figure S22. Power-time curve for 3HBA form II dissolution in DMSO.

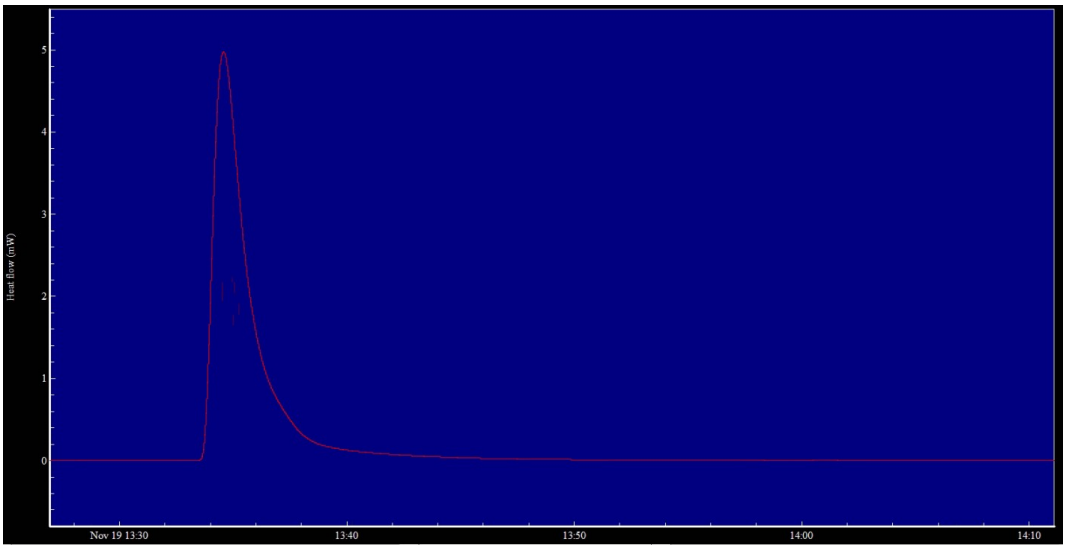

Figure S23. Power-time curve for 3HBA form III dissolution in DMSO.

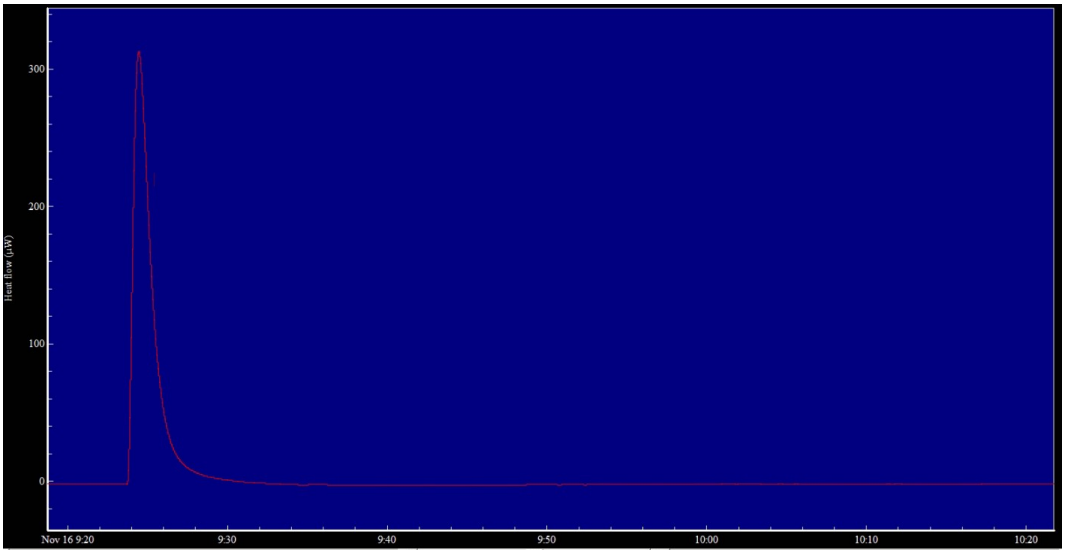

Figure S24. Power-time curve for empty cartridge (blank value) in DMSO.

2.6 Semi-schematic energy temperature diagram

The thermodynamic relationship of the 3HBA polymorphs is displayed in a semi-schematic energy/temperature diagram (Figure S25). Based on the data (DSC and solution calorimetry measurements) it can be concluded that the polymorphic pairs I/II and I/III are monotropically related and that form I is the stable polymorph in the entire temperature range. Based on the data it is not possible to derive whether the polymorphic pair II/III is monotropically or enantiotropically related, although it might be assumed that II/III exhibits a monotropic relationship.

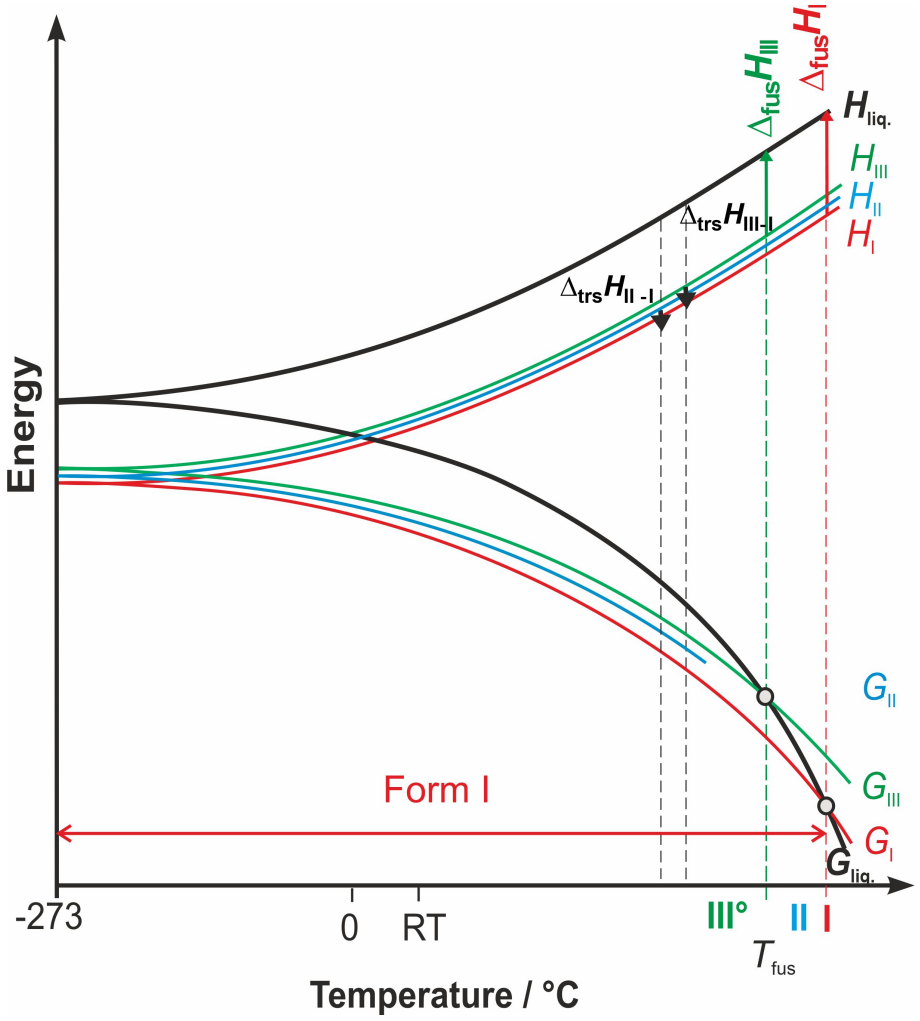

Figure S25. Semi-schematic energy/temperature diagram of 3HBA polymorphs. T_{fus} = melting point, G = Gibbs free energy, H = enthalpy, $\Delta_{fus}H$ = enthalpy of fusion, T_{trs} – transition point, $\Delta_{trs}H$ = transition enthalpy, liq. = liquid phase (melt).

2.7 Variable temperature IR spectroscopy

The form II to I and form III to I phase transformations seen in the DSC heating curves were confirmed using variable temperature IR spectroscopy. The IR spectra were recorded for form II and III every 2 °C from RT to 190 °C.

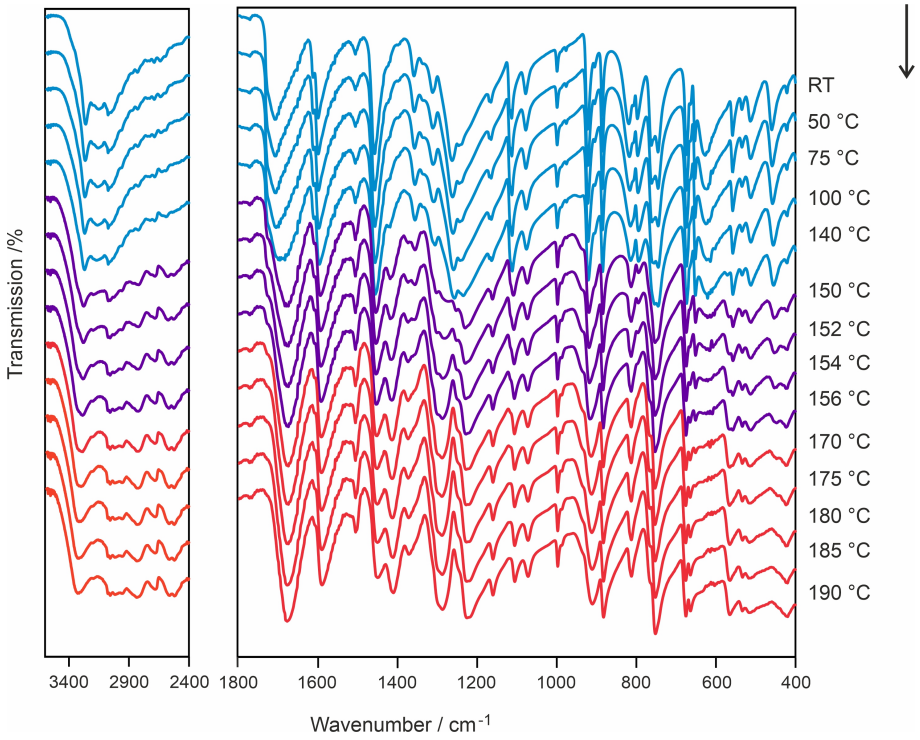

Figure S26. Variable temperature IR spectroscopy following the form II (blue) to form I (red) transformation upon heating. The experiment was stated at room temperature (RT). The temperature at which each of the spectrum was recoded is given on the right-hand side.

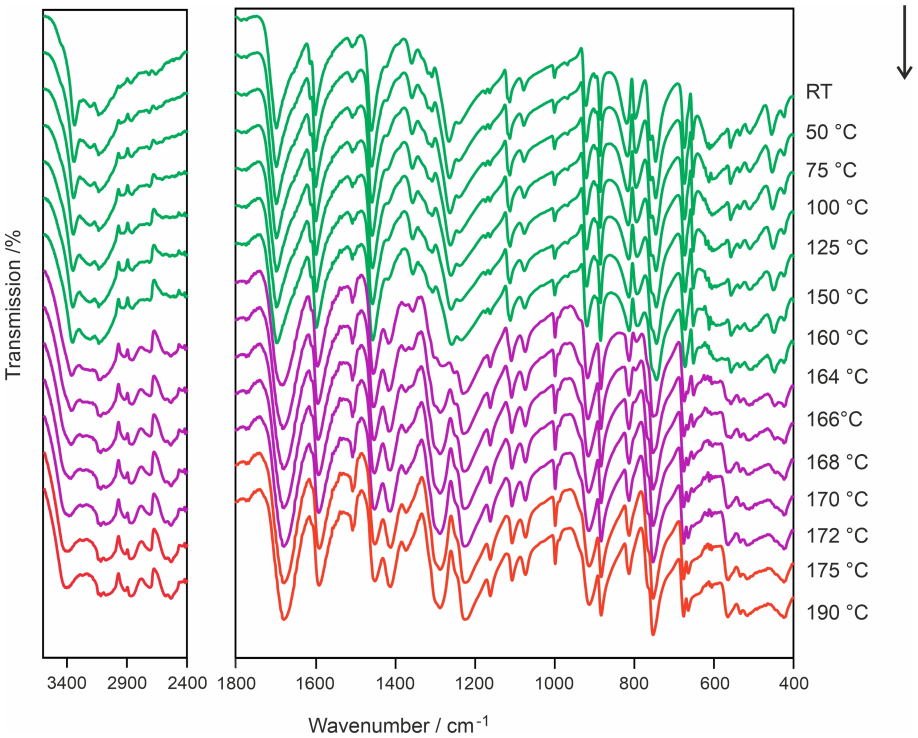

Figure S27. Variable temperature IR spectroscopy following the form III (green) to form I (red) transformation upon heating. The experiment was stated at room temperature (RT). The temperature at which each of the spectrum was recoded is given on the right-hand side.

3 REFERENCES

1. Karamertzanis, P. G.; Pantelides, C. C., Ab initio crystal structure prediction-I. Rigid molecules. *J Comput Chem* **2005,** *26* (3), 304-324.
2. Karamertzanis, P. G.; Pantelides, C. C., Ab initio crystal structure prediction. II. Flexible molecules. *Molecular Physics* **2007,** *105* (2-3), 273-291.
3. Habgood, M.; Sugden, I. J.; Kazantsev, A. V.; Adjiman, C. S.; Pantelides, C. C., Efficient Handling of Molecular Flexibility in Ab Initio Generation of Crystal Structures. *J. Chem. Theory Comput* **2015,** *11* (4), 1957-1969.
4. Breneman, C. M.; Wiberg, K. B., Determining Atom-Centered Monopoles From Molecular Electrostatic Potentials - The Need For High Sampling Density in Formamide Conformational-Analysis. *Journal of Computational Chemistry* **1990,** *11* (3), 361-373.
5. Price, S. L.; Leslie, M.; Welch, G. W. A.; Habgood, M.; Price, L. S.; Karamertzanis, P. G.; Day, G. M., Modelling organic crystal structures using distributed multipole and polarizability-based model intermolecular potentials. *Physical Chemistry Chemical Physics* **2010,** *12* (30), 8478-8490.
6. Stone, A. J., Distributed multipole analysis: Stability for large basis sets. *Journal of Chemical Theory and Computation* **2005,** *1* (6), 1128-1132.
7. Stone, A. J. *GDMA: A Program for Performing Distributed Multipole Analysis of Wave Functions Calculated Using the Gaussian Program System*, 2.2; University of Cambridge: Cambridge, United Kingdom, 2010.
8. Coombes, D. S.; Price, S. L.; Willock, D. J.; Leslie, M., Role of Electrostatic Interactions in Determining the Crystal Structures of Polar Organic Molecules. A Distributed Multipole Study. *Journal of Physical Chemistry* **1996,** *100* (18), 7352-7360.
9. Kazantsev, A. V.; Karamertzanis, P. G.; Adjiman, C. S.; Pantelides, C. C., Efficient Handling of Molecular Flexibility in Lattice Energy Minimization of Organic Crystals. *J. Chem. Theory Comput* **2011,** *7* (6), 1998-2016.
10. Frisch, M. J.; Trucks, G. W.; Schlegel, H. B.; Scuseria, G. E.; Robb, M. A.; Cheeseman, J. R.; Scalmani, G.; Barone, V.; Petersson, G. A.; Nakatsuji, H.; Li, X.; Caricato, M.; Marenich, A. V.; Bloino, J.; Janesko, B. G.; Gomperts, R.; Mennucci, B.; Hratchian, H. P.; Ortiz, J. V.; Izmaylov, A. F.; Sonnenberg, J. L.; Williams; Ding, F.; Lipparini, F.; Egidi, F.; Goings, J.; Peng, B.; Petrone, A.; Henderson, T.; Ranasinghe, D.; Zakrzewski, V. G.; Gao, J.; Rega, N.; Zheng, G.; Liang, W.; Hada, M.; Ehara, M.; Toyota, K.; Fukuda, R.; Hasegawa, J.; Ishida, M.; Nakajima, T.; Honda, Y.; Kitao, O.; Nakai, H.; Vreven, T.; Throssell, K.; Montgomery Jr., J. A.; Peralta, J. E.; Ogliaro, F.; Bearpark, M. J.; Heyd, J. J.; Brothers, E. N.; Kudin, K. N.; Staroverov, V. N.; Keith, T. A.; Kobayashi, R.; Normand, J.; Raghavachari, K.; Rendell, A. P.; Burant, J. C.; Iyengar, S. S.; Tomasi, J.; Cossi, M.; Millam, J. M.; Klene, M.; Adamo, C.; Cammi, R.; Ochterski, J. W.; Martin, R. L.; Morokuma, K.; Farkas, O.; Foresman, J. B.; Fox, D. J. *Gaussian 16 Rev. C.01*, Wallingford, CT, 2016.
11. Anghel, A. T.; Day, G. M.; Price, S. L., A study of the known and hypothetical crystal structures of pyridine: why are there four molecules in the asymmetric unit cell? *CrystEngComm* **2002,** *4* (62), 348-355.
12. Day, G. M.; Price, S. L.; Leslie, M., Elastic constant calculations for molecular organic crystals. *Crystal Growth & Design* **2001,** *1* (1), 13-27.

13. Day, G. M.; Price, S. L.; Leslie, M., Atomistic calculations of phonon frequencies and thermodynamic quantities for crystals of rigid organic molecules. *Journal of Physical Chemistry B* **2003,** *107* (39), 10919-10933.
14. Chisholm, J. A.; Motherwell, S., COMPACK: a program for identifying crystal structure similarity using distances. *Journal of Applied Crystallography* **2005,** *38*, 228-231.
15. Rohlicek, J.; Skorepova, E.; Babor, M.; Cejka, J., CrystalCMP: an easy-to-use tool for fast comparison of molecular packing. *J. Appl. Crystallogr.* **2016,** *49* (6), 2172-2183.
16. Turner, M. J.; Grabowsky, S.; Jayatilaka, D.; Spackman, M. A., Accurate and Efficient Model Energies for Exploring Intermolecular Interactions in Molecular Crystals. *J. Phys. Chem. Lett.* **2014,** *5* (24), 4249-4255.
17. Turner, M. J.; Thomas, S. P.; Shi, M. W.; Jayatilaka, D.; Spackman, M. A., Energy frameworks: insights into interaction anisotropy and the mechanical properties of molecular crystals. *Chem. Commun.* **2015,** *51* (18), 3735-3738.
18. Mackenzie, C. F.; Spackman, P. R.; Jayatilaka, D.; Spackman, M. A., CrystalExplorer model energies and energy frameworks: extension to metal coordination compounds, organic salts, solvates and open-shell systems. *IUCrJ* **2017,** *4* (5).
19. Clark, S. J.; Segall, M. D.; Pickard, C. J.; Hasnip, P. J.; Probert, M. J.; Refson, K.; Payne, M. C., First principles methods using CASTEP. *Zeitschrift fur Kristallographie* **2005,** *220* (5-6), 567-570.
20. Perdew, J. P.; Burke, K.; Ernzerhof, M., Generalized gradient approximation made simple. *Physical Review Letters* **1996,** *77* (18), 3865-3868.
21. Vanderbilt, D., Soft Self-Consistent Pseudopotentials in a Generalized Eigenvalue Formalism. *Physical Review B* **1990,** *41* (11), 7892-7895.
22. Tkatchenko, A.; Scheffler, M., Accurate Molecular Van Der Waals Interactions from Ground-State Electron Density and Free-Atom Reference Data. *Phys. Rev. Lett* **2009,** *102* (7), 073005/1-073005/4.
23. Markvardsen, A. J.; David, W. I. F.; Johnson, J. C.; Shankland, K., A probabilistic approach to space-group determination from powder diffraction data. *Acta Crystallogr. , Sect. A: Found. Crystallogr* **2001,** *A57* (1), 47-54.
24. David, W. I. F.; Shankland, K.; van de Streek, J.; Pidcock, E.; Motherwell, W. D. S.; Cole, J. C., DASH: a program for crystal structure determination from powder diffraction data. *Journal of Applied Crystallography* **2006,** *39*, 910-915.
25. Pawley, G. S., Unit-Cell Refinement from Powder Diffraction Scans. *Journal of Applied Crystallography* **1981,** *14* (DEC), 357-361.
26. Coelho, A., TOPAS and TOPAS-Academic: an optimization program integrating computer algebra and crystallographic objects written in C++. *Journal of Applied Crystallography* **2018,** *51* (1), 210-218.
27. Hempler, D.; Schmidt, M. U.; van de Streek, J., Validation of missed space-group symmetry in X-ray powder diffraction structures with dispersion-corrected density functional theory. *Acta Crystallographica, Section B: Structural Science, Crystal Engineering and Materials* **2017,** *73* (4), 756-766.